Scanning x-ray nano-diffraction on Dictyostelium discoideum: Supplementary information

Marius Priebe*, Marten Bernhardt*, Christoph Blum+, Marco Tarantola+, Eberhard Bodenschatz+, Tim Salditt*[1]

*Institut für Röntgenphysik, Georg-August-Universität Göttingen, Friedrich-Hund-Platz 1, Göttingen, D-37077, Germany,
+Max Planck Institute for Dynamics and Self-Organization, Am Fassberg 17, 37077 Göttingen, Germany

1 X-ray nano-diffraction setup GINIX at P10:

X-ray measurements were performed at the Göttingen Instrument for Nano-Imaging with X-rays (GINIX) (1, 6), at the P10 beamline of the synchrotron radiation source PETRAIII (Desy Photon Science, Hamburg), see also Fig. 1 (a) in the main article. The undulator was operated in the first harmonic. The beam was monochromatized by a Si(111) double crystal monochromator to a photon energy $E_\lambda = 7.9$keV, and focused by a pair of elliptically shaped Kirkpatrick-Baez (KB) mirrors to $326\,nm(h) \times 392\,nm(v)$ (FWHM), with a total photon flux of $I_0 = 1.1 \cdot 10^{11}$ph/s, as measured with the photon counting pixel detector Pilatus 300K (Dectris Ltd, Baden, Switzerland), positioned 5.28m behind the sample, which is placed in the focal plane of the KB. The beam is partially coherent with a global degree of coherence 0.36 and 0.68, in the horizontal and vertical direction, respectively (6). The beam can be made fully coherent by closing the slits in front of the KB, at the expense of lower flux and a focal spot size which broadens by diffraction. Depending on the exact alignment and ring orbit, spot sizes below $200\,nm$ can also be achieved. Of particular importance for the present nano-focus diffraction measurements is the soft-edge tantalum aperture (8) which is placed $3\,mm$ upstream from the focal plane to reduce the background scattering. This aperture with soft edges successfully reduces the background, see the far-field pattern of the empty beam, presented in Fig. 2 (b) in the main article. Importantly, the pronounced streaks of typical KB far-fields are eliminated, which can contaminate the diffraction patterns of the sample.

[1]Corresponding author Tel.: (+49)551-399427, Fax: (+49)551-399430, Email: tsaldit@gwdg.de

As sketched in Fig. 1 (a) in the main article two motorized semi-transparent beamstops (BS) (7) installed in the detector evacuated flight tube are employed to attenuate the direct (primary) beam. A $25\,\mu m$ thick tungsten plate of $8.0\,mm \times 7.0\,mm$ covers the primary beam and a larger silicon plate of $280\,\mu m$ thickness measuring $17.1\,mm \times 12.0mm$ attenuates a larger area around the central beam. The effect of the two beamstops is readily inspected in the far-field pattern shown in Fig. 2 (b) in the main article.

A xyz piezo stage (PI) is used to scan the samples in the beam. Scanning can be performed stepwise through the beam. Typical step sizes were $250\,nm$ to $2\mu m$, depending on the scan, typical dwell times were between $0.05\,s$ and 0.5 s. At each position a full diffraction pattern is recorded. Step sizes can be set separately for the columns and lines. For fast scanning which is particularly important for radiation sensitive samples, a continuous scanning mode is used. Here, linewise scanning is perfomed such that the motion is continuous along the lines. The detector readout is triggered according to the desired resolution along the line. An inline optical microscope (Maatel), positioned directly behind the sample, is used to identify the region of interest (ROI) on the sample and position it with respect to the beam, see Fig. 1 (e). To protect the sample from radiation damage, a 100K environment is provided by a N_2 cryostream (Oxford Cryosystems Ltd, Oxford, United Kingdom), as sketched in Fig. 1 (a) in the main article. A fast shutter triggered to the detector also helps to prevent unnecessary radiation exposure. Sample holders with magnetic bases and transfer vials are used to safely position the samples in the beam.

2 Preparation protocols

2.1 Materials

HL5 medium: contains $7g/l$ yeast extract, $14g/l$ protease peptone, $0.5g/l$ KH_2PO_4, $0.5g/l$ $Na_2HPO_4 \times H_2O$, $13.5\,g/l$ glucose (HLG0101, Formedium)
Phosphate buffered saline solution "Sorensen buffer": $14.7\,mM$ KH_2PO_4 and $2\,mM$ Na_2HPO_4.
The buffer is adjusted to pH 6.0.
Formaldehyde fixation solution: 37 % formaldehyde in water with 10 % methanol (stock solution by Merck, Darmstadt, Germany) and PBS
The stock solution is diluted in PBS to a final formaldehyde concentration of 4 %.

2.2 Cell lines:

We used *D. discoideum* of the axenic cell line AX2-214 with a green fluorescent protein (GFP) fused to the LimE-protein (2), a component of the Arp2/3-complex, which acts as a selective marker for filamentous actin polymerization (3). Thus the actin components of the cytoskeleton, i. e. pseudopodia and the actin myosin cortex can be visualized by fluorescence microscopy of a second set of samples. The second line of cells, used in Fig. 7 (c) in the main article is derived from the same stem, but the LimE-protein carries a monomeric Red Fluorescent Protein and a GFP is fused to the myosin-II motor proteins. The cells are grown in HL5 medium. For preparation of chemotactic competent cells, *D. discoideum* cells are washed with Sorensen buffer twice and resuspended in Sorensen buffer to a concentration of $2 \cdot 10^6$ cells per ml.

2.3 Cell preparation

Preparation of chemotactically competent cells: We follow the protocol described in (9): The preparation of chemotactically competent cells, so called 'pulsing', starts one day prior to the experiment being carried out. An inoculum of $1 \cdot 10^6$ cells is pipetted into 25 ml HL5 medium and cultivated at 22°C as a shaking culture (150 rpm). 7 hours in advance of the experiment the full shaking culture is centrifuged (1000 rpm, 3 min, 4°C), washed once in phosphate buffer (PBS, pH = 6) and the remaining pellet is diluted in 20 ml PBS. This new shaking culture (150 rpm, 22°C) is subject to periodic pulses of 3-5 cyclic adenosine monophosphate (cAMP, Sigma-Aldrich) in order to enhance the development of the D. discoideum amoebae (10). A pulse of cAMP consists of approximately 60 μl with a concentration of 18 μM and is added every 6 minutes. The cells **develop** for 5 hours. 1 hour prior to the further preparation the cells are washed 1 - 3 times in PBS (1000 rpm, 3 min, 4°C) and are finally dispersed in 10 ml PBS (depending on the cell density). This cell solution is then ready to be processed in the following preparation protocols except for the microfluidic chambers.

Frozen hydrated cells: Silicon nitride (Si_3N_4) membranes (Silson Ltd., Northampton, UK) are rendered hydrophilic in a plasma cleaner for 10 Minutes, and are then placed in a petridish with PBS. A drop of the cell suspension is gently pipetted onto the membrane and the cells are allowed to adhere, Fig. 1 (a). As soon as the cells show a state of high motility, as inspected by optical microscopy (Zeiss Observer Z1), the membrane is trans-

ferred to the temperature and humidity controlled preparation chamber of a gridplunger (Leica GP2 (4, 5)). A layer of PBS is always present on the membrane to prevent the cells from drying out (middle). Under inspection of a binocular microscope, the liquid is blotted inside of the preparation chamber followed by the fast injection into liquid ethane just above its boiling point (−184°C). The fast cooling rate ensures vitrification of the water inside the cells. The samples are constantly kept at liquid nitrogen temperatures, thus well below the glass transition temperature. The samples are brought to a storage vessel, where they are kept in a liquid nitrogen bath, see Fig. 1 (a).

Freeze dried cells: Freeze dried cells are prepared from frozen hydrated cells, using a home built freeze drier. The samples are passively cooled using a massive copper block installed at liquid nitrogen temperature in a large high vacuum vessel, over a time of 60 hours. The temperature of the sample slowly increases before the chamber is vented with dry nitrogen. After a further 12 hours under dry nitrogen atmosphere for slow temperature equilibration, samples are taken out. The samples are transferred to a vacuum desiccator to protect them from ambient humidity.

Chemically fixed cells: The living, motile cells are left on the substrate under PBS until they reached a state of high motility. The PBS is then carefully replaced with the formaldehyde fixation solution. The fixation solution is left for 15 minutes before the substrate is gently rinsed and afterwards stored under pure PBS again. Fixated cells are stored at 4°C.

Microfluidic chambers for living cells: Living cells were measured in x-ray compatible microfluidic devices (ibidi GmbH, Munich, Germany). As illustrated in Fig. 1 (c), two transparent polymer slides form top and bottom and carry a spacer of $50\mu m$ in between. The channel is defined by a $5\,mm$ wide and $50\,mm$ long slit in the spacer. Silicon nitride windows (membrane thickness $1\,\mu$m) are fitted into the channel floor and top to reduce background scattering. The channels are accessible by a connection port (Luer) on each end of the channel. A photograph of the chamber taken during experiments is shown in Fig. 1 (d), with the chamber outlined in red. To prevent formation of gas bubbles, the PBS was degased by placing it in an ultrasonic bath for 10 minutes while at the same time a vacuum pump was connected to the PBS container. For preparation the channels are filled with PBS, then cells are washed from their substrate and the suspension is

filled in the channel. Cells are allowed to adhere for at least ten minutes before the channel is flushed with at least 3 times the volume of the channel of degased PBS to remove dead or non adhering cells. The channel outlets are sealed with plugs and the sample is mounted on the stage.

2.4 Cryogenic sample handling

Various aspects of the preparation protocol and the sample environment at the beamline are illustrated in Fig. 1 including:

(a) the plunge freezing process, as described in section 2.3.

(b) the transfer of cryogenic samples: consists of safely fixing the sample onto a specialized magnetic goniometer base which can then be transported in a liquid nitrogen filled transfer vial up to one minute. The vial is not removed until the sample is safely placed in the sweet spot of the cryostream such that after removal of the vial it is directly cooled by the cryostream. Finally the goniometer base is attached to its counterpart on the sample stage without the sample leaving the cryostream.

(c) Sketch and photo (d) of the the live cell imaging chamber: The channel consists of a slit in a spacer which is sealed by two plates. Silicon nitride windows have been integrated into both plates to reduce background scattering. Microfluidic ports (Luer slip female) in the top slide allow easy access to the channel that measures $h \times w \times l = 50\,\mu m \times 5\,mm \times 50\,mm$. The photo shows the chamber (outlined in red) during the experiments at the GINIX, where it has been mounted on the piezo sample tower.

(e) micrographs of *D. discoideum* cells, from left to right: as imaged in a cryogenic visible light microscope just after the preparation, inline optical microscope used at the beamline for alignment, along with the corresponding x-ray dark-field map. All three control instances ensure a high quality and consistency of the samples as cells can be inspected and indexed before the synchrotron beamtime. The diffraction experiments are performed on the cells chosen before, which allows a correlation of the diffraction pattern with the optical light microscope. The darkfield map confirms the positioning.

H

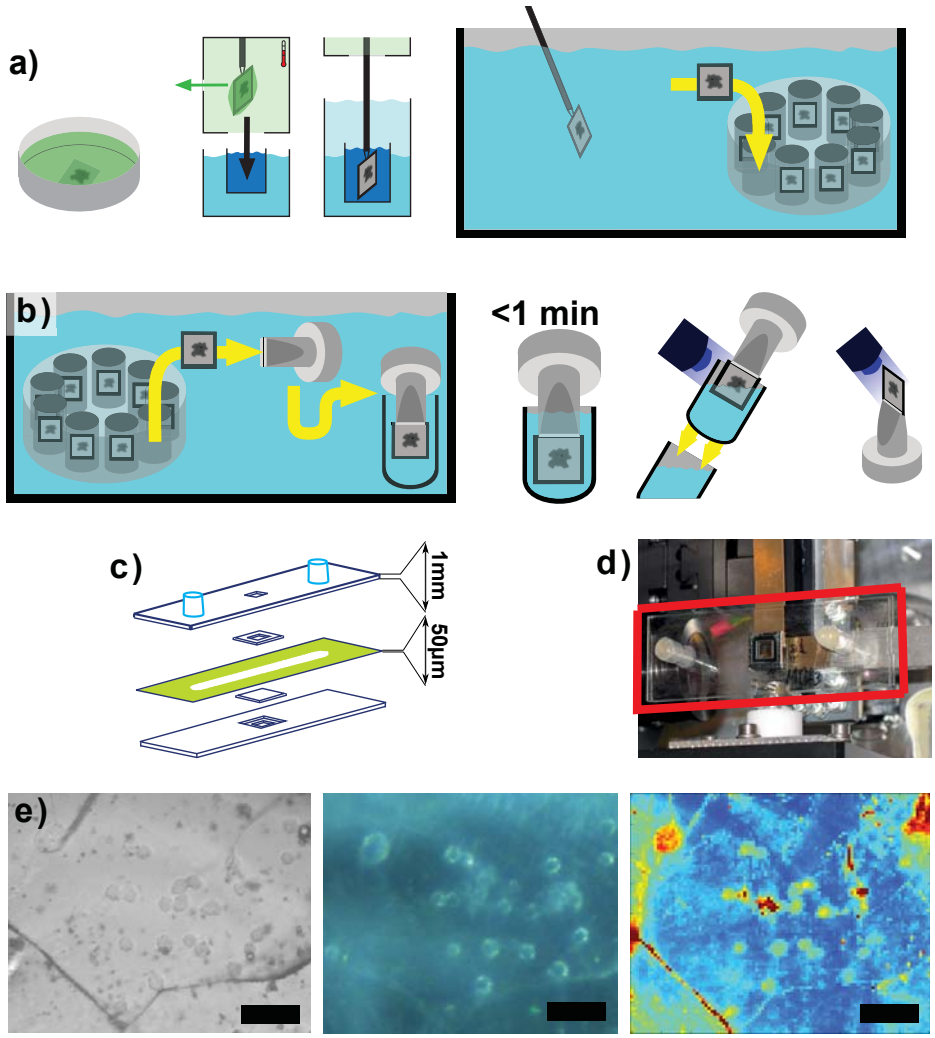

Figure 1: (**a**) Illustration of cryoplunging process, (**b**) the mounting procedure of cryogenic samples, (**c**) schematic of a microfluidic chamber used for measuring initially living cells, (**d**) photograph of the transparent microfluidic chamber (outlined in red) installed at the GINIX. (**e**) Images of a frozen hydrated sample: (left) Micrograph made with a cryogenic bright field light microscope in Köhler illumination. (middle) Same sample area as seen by the inline microscope at the GINIX setup in transmission illumination. (right) Corresponding x-ray darkfield contrast of same region. The scalebar correspond to 40μm.

3 Simulated fibre diffraction and reciprocal space transformation

In the simulation presented in Sec. 3 of the main article, the necessary transformation of the reciprocal space associated with the fibre bundles to that of the laboratory frame is handled as follows. We first consider a fibre axis which is inclined at an angle ϑ with respect to the optical axis. Hence, for $\vartheta = 0°$ the diffraction pattern would correspond to a cut through the azimuthal plane in reciprocal space Q_X, Q_Y reflecting the two-dimensional structure factor $SF(Q_x, Q_y)$ calculated from the filament positions $\mathbf{R_j}$. This could correspond to an ordered 2d liquid or a crystalline arrangement, such as a 2d cubic or hexagonal pattern, depending on the physical situation. For $\vartheta = 90°$, the fibre axis is perpendicular to the optical axis along a radial line on the detector perpendicular to the streak and forming an angle χ with respect to the q_z axis. Along with a rotation around the fibre axis φ the fibre bundles orientation is fully specified by the parameters χ, ϑ, φ.

We first apply a rotation $\mathcal{R}^x_\chi$ of the detector frame around the optical axis (x, q_x) in order to obtain the detector axis $q\prime_z$ intersecting with the plane suspended by the fibre axis and the optical axis, i. e.

$$\begin{pmatrix} q\prime_y \\ q\prime_z \end{pmatrix} = \begin{pmatrix} \cos\chi & \sin\chi \\ -\sin\chi & \cos\chi \end{pmatrix} \begin{pmatrix} q_y \\ q_z \end{pmatrix} . \tag{1}$$

From $(q\prime_y, q\prime_z)$, the components of the momentum transfer vertical and perpendicular to the fibre axis are easily obtained according to

$$Q_z = q\prime_z \sin\vartheta \tag{2}$$
$$Q_\parallel = (q\prime_y^2 + q\prime_z^2 \cos^2\vartheta)^{0.5} , \tag{3}$$

and finally by rotation $\mathcal{R}^Z_\phi$ around the fibre axis the components in the fibre coordinate system required for the structure factor

$$Q_x = Q_\parallel \cos\phi \tag{4}$$
$$Q_y = Q_\parallel \sin\phi . \tag{5}$$

4 Definition of masks for STXM contrasts

The quantitative and qualitative results of the STXM contrasts depend considerably on the masks, that were applied during the calculation. It mainly defines the region (beam mask) where the primary beam can be found and the region where scattering events occur (darkfield mask).

The DPCy (like the DPCz, wich we do not show in this paper) depends on the choice of the beam mask, as the center of mass is determined with respect to the pixels within the beam mask. Including the right slope of the primary beam is necessary to accurately track the center of mass of the intensity, but is compromised by the different intensity levels on and off the inner beamstop. This would require **rescaling** the detector image in order to reconstruct the full beam profile without attenuation artefacts.

The darkfield contrast is calculated by applying the darkfield mask on the far-field intensity distribution and summing up the remaining intensity to obtain I_{scatt}. We divide I_{scatt} by the intensity of the primary beam I_0 (determined with the pilatus) to obtain the relative scattered intensity $\frac{I_{scatt}}{I_0}$ which is used in the darkfield maps. Variations of I_0 (e. g. due to changes in the synchrotron ring current) are not accounted for, as these variations are typically in the order of $\sim 1\%$. The darkfield mask is defined as the inverse of the beam mask. The intensity from mirror scattering can be cut out at the price of **losing** scattered photons at the very small q_r. As it mainly adds a constant contribution to the relative scattered intensity the values are shifted while the contrast and dynamic range are little affected.

5 Additional STXM maps

Additional maps of a STXM scan are shown in Fig. 3.

References

1. Kalbfleisch, S., H. Neubauer, S. P. Krüger, M. Bartels, M. Osterhoff, D. D. Mai, K. Giewekemeyer, B. Hartmann, M. Sprung, and T. Salditt, 2011. The Göttingen Holography Endstation of Beamline P10 at PETRA III/DESY *AIP Conf. Proc.* 1365:96–99.

2. Schneider, N., I. Weber, J. Faix, J. Prassler, A. Müller-Taubenberger, J. Köhler, E. Burghardt, G. Gerisch, and G. Marriott, 2003. Lim Protein Involved in the Progression of Cytokinesis and Regulation of the Mitotic Spindle *Cell Motility and the Cytoskeleton* 56:130–139

3. Diez, S., G. Gerisch, K. Anderson, A. Müller-Taubenberger, and T. Bretschneider, 2005. Subsecond reorganization of the actin network in cell motility and chemotaxis *PNAS* 102:7601–7606.

4. Resch, G. P., M. Brandstetter, A. M. Pickl-Herk, L. Königsmaier, V. I. Wonesch, and E. Urban, 2011. Immersion Freezing of Biological Specimens: Rationale, Principles, and Instrumentation *Cold Spring Harbor Protocols* doi:10.1101/pdb.top118

5. Resch, G. P., M. Brandstetter, V. I. Wonesch, and E. Urban, 2011. Immersion Freezing of Cell Monolayers for Cryo-Electron Tomography *Cold Spring Harbor Protocols* doi:10.1101/pdb.prot5643

6. Salditt, T., S. Kalbfleisch, M. Osterhoff, S. P. Krüger, M. Bartels, K. Giewekemeyer, H. Neubauer, and M. Sprung, 2011. Partially coherent nano-focused x-ray radiation characterized by Talbot interferometry *Opt Express* 19(10):9656-9675

7. Wilke, R. N., M. Vassholz, and T. Salditt, 2013. Semi-transparent central stop in high-resolution X-ray ptychography using KirkpatrickBaez focusing *Acta Cryst. A* 69:490497

8. Takahashi, Y., A. Suzuki, N. Zettsu, Y. Kohmura, Y. Senba, H. Ohashi, K. Yamauchi, and T. Ishikawa, 2011. Towards high-resolution ptychographic x-ray diffraction microscopy *Phys. Rev. B* 83:214109

9. Westendorf, C., 2013. PhD thesis: Oscillatory dynamics of the actin cytoskeleton Georg-August-Universität Göttingen

10. Chisholm, R., S. Hopkinson, and H. Lodish, (1987). Superinduction of the Dictyostelium discoedium cell surface cAMP receptor by pulses of cAMP *PNAS* 84(4):10301034

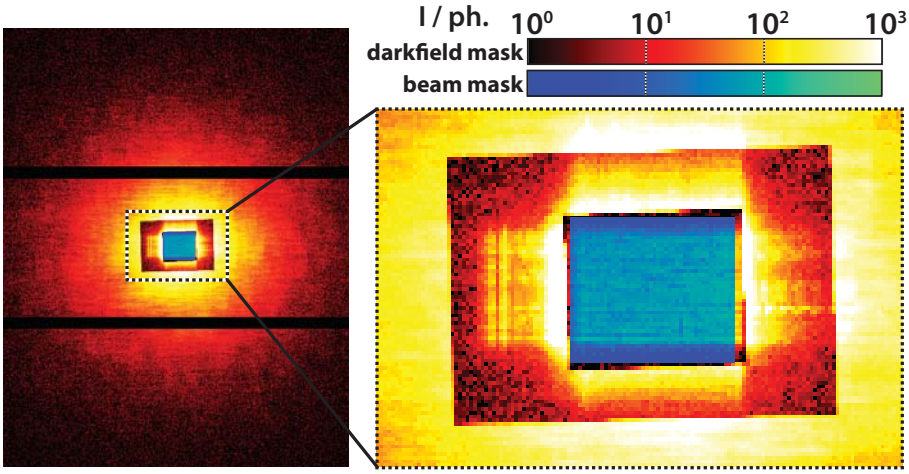

Figure 2: An exemplary diffraction pattern is shown here to illustrate the masks that are applied in the STXM contrasts. The darkfield mask is displayed in a red color scheme and the beam mask, which is defined as the inverse of the darkfield mask, is represented in a blue to green color code. The darkfield mask covers the whole detector image exept for the area of the primary beam, as becomes clearer in the inset. The challenge in the choice of masks is that the central beam is very close to the right side of the inner beamstop and thus cannot be fully framed without considering signal that passed through different absorbers. In this case the different intensity levels would cause an unrealistically high contrast.

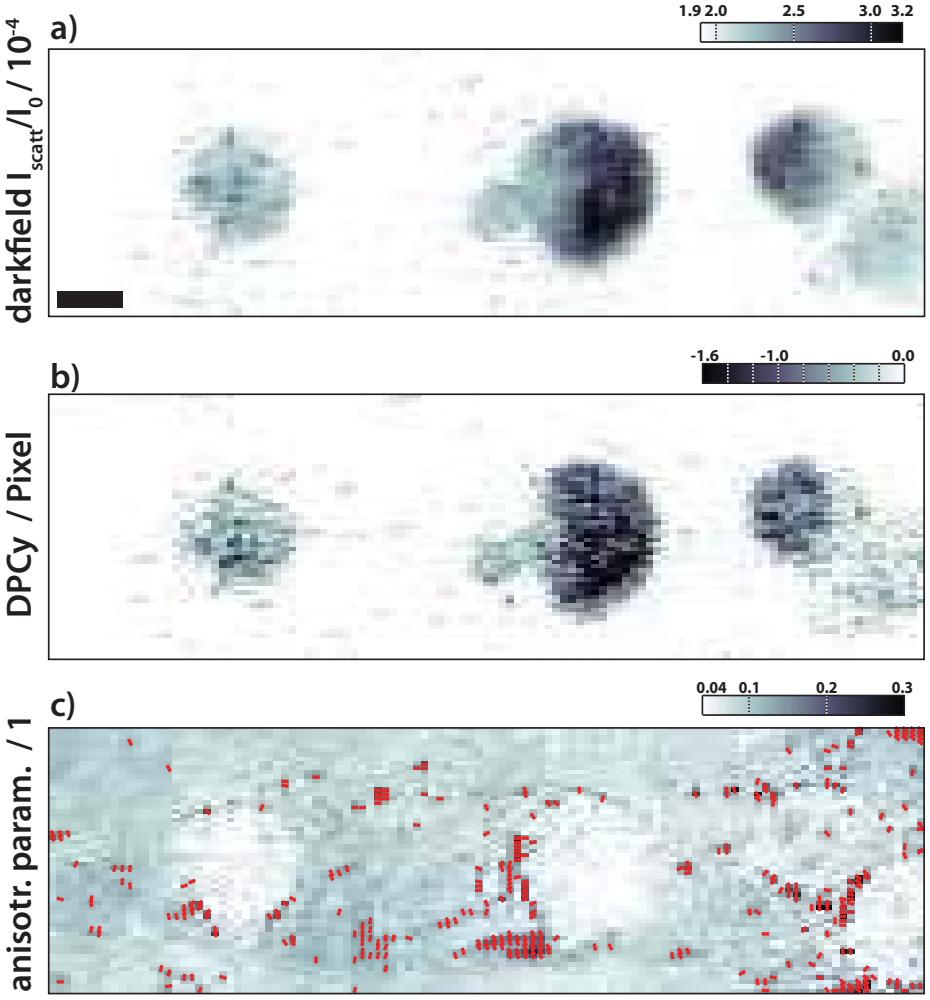

Figure 3: **(a)** Darkfield map, **(b)** DPCy map and **(c)** streak finder map of another STXM scan on frozen hydrated *D. discoideum* cells. The specific set of cells shows very weak signals in all three contrasts. Here, the central cell is of special interest, showing only weak scattering and weak anisotropy, which is still pronounced around the protrusion. The measurement was performed at the GINIX with $I_0 = 1.1 \cdot 10^{11}$ph/s and 0.*e*s exposure per data point. The scale bar denotes 5 μm.